

# Spin-selective electron transfer in quantum dot array

Shumpei Masuda\*,<sup>1</sup> Kuan Yen Tan,<sup>1</sup> and Mikio Nakahara<sup>2</sup>

<sup>1</sup>*QCD Labs, Department of Applied Physics,*

*Aalto University, Aalto 00076, Finland*

<sup>2</sup>*Research Center for Quantum Computing and Department of Physics,*

*Kindai University, Higashi-Osaka, 577-8502, Japan*

\* *shumpei.masuda@aalto.fi*

## Abstract

We propose a spin-selective coherent electron transfer in a silicon-quantum-dot array. Oscillating magnetic fields and temporally controlled gate voltages are utilised to separate the electron wave function into different quantum dots depending on the spin state. We introduce non-adiabatic and adiabatic protocols which offer fast electron transfer and the robustness against the error in the control-field pulse area, respectively. We also study a shortcut-to-adiabaticity protocol which compromises these two protocols. We show that this scheme can be extended to multi-electron systems straightforwardly and used for non-local manipulations of the electrons.

## INTRODUCTION

Spins in silicon-based quantum dots offer a promising platform for fault-tolerant quantum information processing [1]. Fidelities of readout and single-qubit control above the surface code threshold [2] have exhibited exceptionally long lifetimes [3–5] and coherence times [6–9], two figure-of-merits that are desirable for quantum computing. Various types of qubit operations have been demonstrated [10, 11] including two-qubit logic gates using the exchange interaction between single spins in isotopically enriched silicon [12]. On the other hand, single electron pumps [13–19] and the shuttling of single electron [20, 21] in quantum dots have also been demonstrated at metrological accuracy. In fact, single-spin shuttling in a GaAs system quantum dot array has recently been demonstrated using this shuttling operation, and has been shown to preserve the spin coherence up to macroscopic distances [21].

In cold atom systems, the coherent transport of neutral atoms [22] and the creation of highly-entangled states of neutral atoms have been demonstrated utilising the hyperfine spin-dependent optical lattice potentials [23]. Two-qubit gate operations employing such state-dependent potentials have been studied theoretically [24–26]. To the best of our knowledge, however, no spin-selective electron transfer which offers non-local qubit operations in a quantum dot array has been demonstrated.

In this report, we propose a scheme for spin-selective coherent electron transfer in a quantum dot array achievable using the proven experimental techniques in single-spin shuttling [20, 21] in a silicon qubit architecture [10–12]. The gradient of oscillating magnetic fields and controlled gate voltages are utilised to separate the electron wave function into different quantum dots in a spin-selective manner. We propose non-adiabatic and adiabatic protocols. The non-adiabatic transfer is fast but also relatively sensitive to the error in timing and amplitude of the control field. Our adiabatic protocol is based on stimulated Raman adiabatic passage (STIRAP) which is a well-known, efficient protocol for state-to-state population transfer [27–29]. We introduce the spin-selective STIRAP (spin-STIRAP) which provides robustness against the errors although the operation time is longer than that of the non-adiabatic protocol. We also examine a non-adiabatic electron transfer based on a shortcut-to-adiabaticity protocol [30, 31] which is referred to as the invariant-based engineering protocol [32]. It is faster than the spin-STIRAP and more robust against the

error of the control field than the simple non-adiabatic protocol. Furthermore, we show that this scheme can be extended to multi-electron systems to implement two-qubit gates. We propose non-local phase manipulations of the electrons as an example.

## SPIN-SELECTIVE ELECTRON TRANSFER

We first consider a four-dot system shown in Fig. 1a, where three quantum dots align along the  $z$ -axis, and a wider quantum dot is located parallel to the array in the  $yz$ -plane. The heights of the potential barriers between the dots and the depths of the potential wells are tunable. There is a stationary uniform magnetic field  $\mathbf{B}_z = (0, 0, B_z)$  parallel to the two-dimensional electron gas. A conducting lead carries the AC currents,  $I_k$  ( $k = p, S$ ), which induce the AC magnetic fields,  $\mathbf{B}_k = (B_k, 0, 0)$ , perpendicular to the two-dimensional electron gas. The conducting lead is separated from Dot 4 by distance  $r_l$ , and is tilted with respect to the dot array by angle  $\theta_l$  to enhance the influence of the spatial dependence of the magnetic field  $\mathbf{B}_k$  on the electron in the quantum dots. This spatial dependence of the magnetic field plays an essential role in our scheme.

We consider spin-selective electron transfer from Dot 1 to Dot 3 in which only the spin-down electron is transferred, while spin-up electron remains in Dot 1. We assume that the electron is initially trapped in Dot 1 and that the state of the electron is a superposition of the lowest-energy spin-up state and the lowest-energy spin-down state.

The electron transfer protocol is illustrated in Fig. 1b. It consists of four steps: (I) adiabatic transfer of the electron to Dot 4, (II) non-adiabatic or adiabatic spin-selective level transfer, (III) adiabatic transfer of the electron to the in-line dots (Dots 1, 2, 3), (IV) loading of the spin-down electron to Dot 3.

In step I, the gate voltages of the in-line dots are gradually increased, and the potential well of Dot 4 is deepened so that the electron is transferred to Dot 4 without energy excitations. In step II, the lowest energy state with spin down is transferred to the second spin-down excited state, while the spin-up electron remains in the spin-up ground state. We use Dot 4 for the level transfer instead of Dot 1 nor the combined dot composed of the in-line dots in order to enhance the influence of the AC magnetic fields to the electron and also to reduce the influence of the fluctuation of the gate voltage at the in-line dots. Three different methods for step II are introduced later. In step III, the barriers of the in-line dots

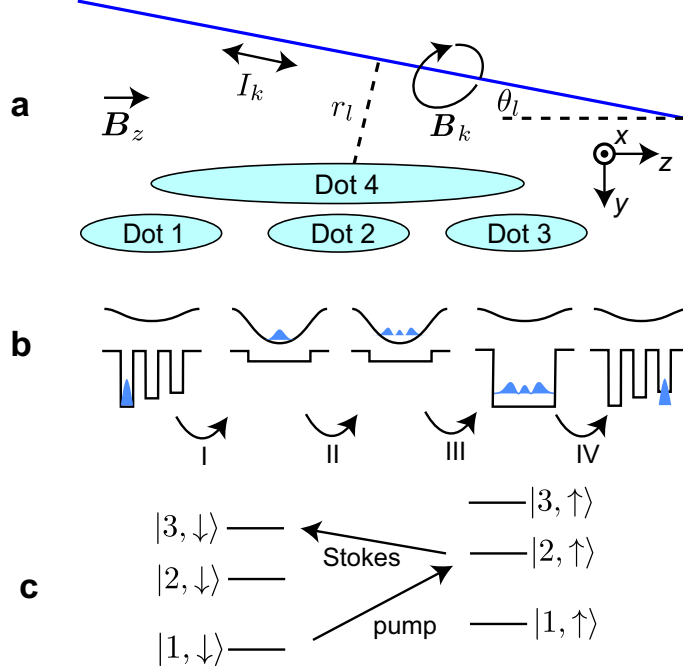


FIG. 1. (a) Schematics of the proposed system. The blue line represents the conducting lead for the AC control currents  $I_k$  ( $k = p, S$ ) producing the magnetic fields  $\mathbf{B}_k = (B_k, 0, 0)$ . The conducting lead is tilted with respect to the dot array by angle  $\theta_l$ . Here,  $r_l$  is the distance of the lead from the center of Dot 4. (b) Schematics of the spin-selective transfer of a single electron. The top black lines represent the potential profile of Dot 4, and the bottom black lines represent the potentials of the dot array. The blue color represents the square of the amplitude of the wave function of the spin-down electron. (c) Energy diagram of the system in step II. Here,  $|i, \uparrow (\downarrow)\rangle$  is the  $i$ th instantaneous eigenstate trapped in Dot 4 with spin up (down). The AC magnetic field  $\mathbf{B}_p$  (pump field) couples  $|1, \downarrow\rangle$  and  $|2, \uparrow\rangle$ , and  $\mathbf{B}_S$  (Stokes field) couples  $|2, \uparrow\rangle$  and  $|3, \downarrow\rangle$ .

are lowered and the potential depth of Dot 4 is reduced so that the electron is adiabatically transferred to the combined dot. In step IV, the barriers of the in-line dots are gradually increased and the depth of the potential wells are tuned so that the Dot 3 has the highest potential of the in-line dots. In the end of step IV, the spin-down electron is carried into Dot 3 because the wave function of the second excited instantaneous eigenstate with spin down is located in Dot 3. On the other hand, the spin-up electron returns to Dot 1. Note that the state of the electron is the superposition of these two states.

The adiabatic transfer of electrons between quantum dots have been routinely used.

Therefore we mainly discuss step II in the following. The duration of step II is much longer than the other steps. Thus, step II dominates the execution time of the transfer process.

Simpler spin-selective electron transfers using only the in-line dots without Dot 4 might be possible if the fluctuation of the gate voltages of the dots and barriers are negligible. However the fluctuation causes the unwanted fluctuation of the separation of the energy levels and thus lowers the transfer efficiency. On the other hand, in our scheme, the electron is prepared in a single dot for adiabatic loading to a selected dot. Thus, we can restrain the influence of the potential fluctuation.

## NON-ADIABATIC AND ADIABATIC SPIN-SELECTIVE LEVEL TRANSFERS

In step II, the electron is trapped in Dot 4. To detail the schemes of step II, we use the energy eigenstates in Dot 4 for  $\mathbf{B}_k = 0$  ( $k = p, S$ ) as a basis of the system. The energy diagram of the system is illustrated in Fig. 1c. Here,  $|i, \downarrow (\uparrow)\rangle$  for  $i = 1, 2, 3$  denote the first three lowest energy levels with spin down (up) in the  $z$ -direction. The energy separations of the levels are not uniform because the potential of Dot 4 is anharmonic. The stationary magnetic field  $\mathbf{B}_z$  causes the Zeeman splitting with energy  $g\mu_B B_z/\hbar$  between spin-up and down states, where  $g$  is the electron  $g$ -factor and  $\mu_B$  is the Bohr magneton.

We aim at a spin-selective transfer in which only spin-down electron is transferred from  $|1, \downarrow\rangle$  to  $|3, \downarrow\rangle$ , while spin-up electron is unaffected. The frequencies  $\omega_k$  of  $\mathbf{B}_k$  are tuned to be  $\omega_p = (E_{2,\uparrow} - E_{1,\downarrow})/\hbar$  and  $\omega_S = (E_{3,\downarrow} - E_{2,\uparrow})/\hbar$ , where  $E_{i,\uparrow(\downarrow)}$  is the energy eigenvalue of  $|i, \uparrow (\downarrow)\rangle$ , so that the pump field  $\mathbf{B}_p$  couples  $|1, \downarrow\rangle$  and  $|2, \uparrow\rangle$ , and the Stokes field  $\mathbf{B}_S$  couples  $|2, \uparrow\rangle$  and  $|3, \downarrow\rangle$ . Note that  $|1, \uparrow\rangle$  is not coupled to the other states by  $\mathbf{B}_k$ .

We represent the effective Hamiltonian of the system using, as a basis, the subset of states  $|1, \downarrow\rangle$ ,  $|2, \uparrow\rangle$  and  $|3, \downarrow\rangle$  coupled by the resonant magnetic fields. The pulsed magnetic fields used in step II are represented as

$$B_k(t, \mathbf{r}) = B_k^{(e)}(t)\eta_k(\mathbf{r})\cos(\omega_k t) \quad (1)$$

with the envelope function  $B_k^{(e)}(t)$ , which is the intensity of the pump and the Stokes field at the center of Dot 4. Here,  $\eta_k(\mathbf{r})$  is the ratio of the intensity of the field at  $\mathbf{r}$  to  $B_k^{(e)}$ . Thus,  $\eta_k(\mathbf{r})$  characterizes the spatial dependence of the magnetic fields. When the AC magnetic fields are sufficiently small, the rotating wave approximation (RWA) holds. Using

the interaction picture and the RWA, the Hamiltonian of the three-level system can be put in the form

$$H_{\text{RWA}}(t) = \frac{\hbar}{2} \begin{pmatrix} 0 & \Omega_p(t) & 0 \\ \Omega_p(t) & 0 & \Omega_S(t) \\ 0 & \Omega_S(t) & 0 \end{pmatrix}, \quad (2)$$

with the Rabi frequencies given by

$$\Omega_k(t) = \frac{B_k^{(e)}(t)g\mu_B\mu_k}{2\hbar}, \quad (3)$$

and with the overlapping factors defined by

$$\begin{aligned} \mu_p &= \int d\mathbf{r} \phi_1^*(\mathbf{r})\eta_p(\mathbf{r})\phi_2(\mathbf{r}), \\ \mu_S &= \int d\mathbf{r} \phi_2^*(\mathbf{r})\eta_S(\mathbf{r})\phi_3(\mathbf{r}), \end{aligned} \quad (4)$$

where  $\phi_i(\mathbf{r}) = \langle \mathbf{r}, \downarrow (\uparrow) | i, \downarrow (\uparrow) \rangle$ . If the magnetic fields  $\mathbf{B}_k$  are spatially uniform, they cannot couple the energy levels because the energy eigenvectors are orthogonal to each other. The spatial dependence of the magnetic fields realizes the coupling between the energy levels.

It has been demonstrated that the valley separation can be tuned via electrostatic gate control of quantum dots providing the splittings spanning 0.3–0.8 meV [82]. Thus, we assume that other valley states are located sufficiently above  $|i, \uparrow (\downarrow)\rangle$ , and multi-valley relaxation effect are negligible. We also assume that the relaxation rate from the excited states  $|2, \uparrow\rangle, |3, \downarrow\rangle$  to the lower energy states induced by the interaction with other electrons is slow enough compared to the duration of step II.

### Non-adiabatic spin-selective electron transfer

One of the non-adiabatic schemes of step II is composed of a  $\pi$ -pulsed pump field followed by a  $\pi$ -pulsed Stokes field that are separated from each other in the time domain as depicted in Fig. 2a. The envelope functions are given as

$$B_k^{(e)}(t) = \begin{cases} B_k^0 & \text{for } |t - T_k| \leq \tau_k/2, \\ 0 & \text{for } |t - T_k| > \tau_k/2, \end{cases} \quad (5)$$

where  $B_k^0$  is the amplitude of the rectangular pulse and  $\tau_k$  is the pulse width. When the pulse areas are  $\pi$ , that is,

$$B_k^0 = \frac{2\pi\hbar}{g\mu_B\mu_k\tau_k}, \quad (6)$$

the state is transferred from  $|1, \downarrow\rangle$  to  $|2, \uparrow\rangle$ . However this scheme is sensitive to the error in the pulse area compared to the adiabatic scheme discussed below. Inaccuracy of the pulse area causes the imperfection of the population transfer.

### Spin-selective STIRAP

Stimulated Raman adiabatic passage (STIRAP) has been widely studied for population transfer of molecules [33–40], transport of single atoms [41–46], electrons [47, 48] and BECs [49–52]. The remarkable properties of this protocol have already been demonstrated in diverse areas such as chemical reaction dynamics [53], laser-induced cooling of atomic gases [54], light beams propagating in three evanescently coupled optical waveguides [55–58], sound propagation in sonic crystals [59] and control of a superconducting qubit [60]. In spin-based quantum computing architecture, this protocol can be utilised to transfer qubits coherently across large distances [61].

Here, we introduce the spin-STIRAP of the electron in Dot 4. The envelope functions of the pump and the Stokes fields are represented as

$$B_k^{(e)}(t) = B_k^0 \exp \left[ -\frac{(t - T_k)^2}{2\sigma^2} \right], \quad (7)$$

where  $\sigma$  is defined by

$$\sigma = \frac{\text{FWHM}}{2\sqrt{2\ln 2}} \quad (8)$$

with the full width at half-maximum (FWHM) and the maximum intensity  $B_k^0$  of the peak centered at  $T_k$ . The separation of the peak is chosen as

$$T_p - T_s = \frac{3\text{FWHM}}{4\sqrt{\ln 2}}. \quad (9)$$

Note that the pump pulse follows the Stokes pulse,  $T_p > T_s$ , as shown in Fig. 2b.

A time-dependent, field-dressed eigenstates of the system, which is a linear combinations of the field-free states, is represented as

$$|\phi_0(t)\rangle = \cos \Theta(t)|1, \downarrow\rangle - \sin \Theta(t)|3, \downarrow\rangle, \quad (10)$$

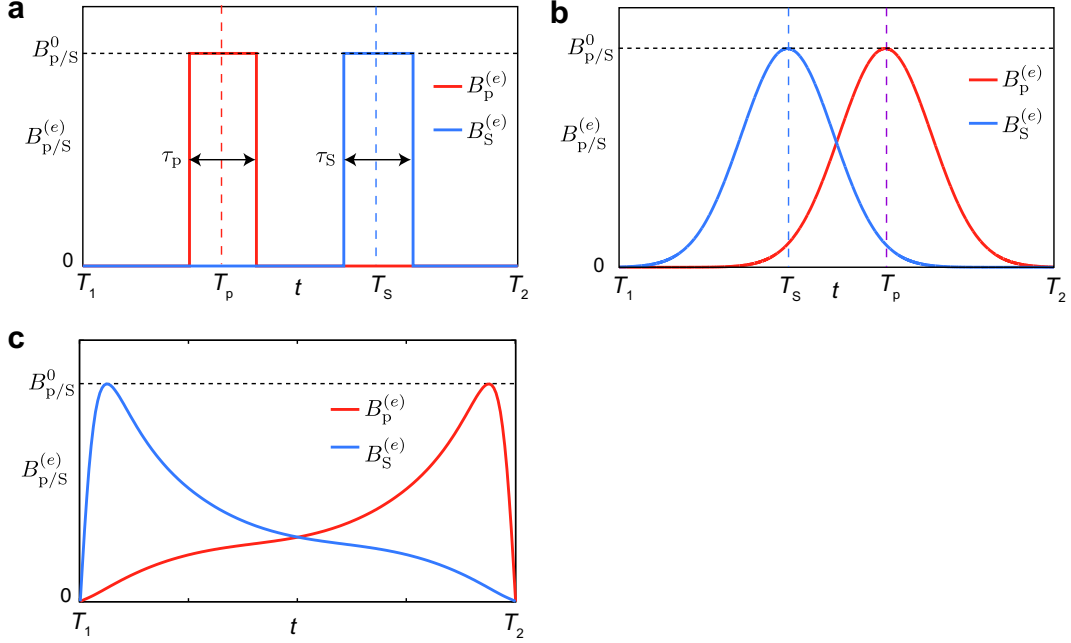


FIG. 2. Schematics of the envelop function of the magnetic fields  $B_p^{(e)}$  and  $B_S^{(e)}$  for (a)  $\pi$ -pulse control, (b) spin-STIRAP and (c) invariant-based engineering protocol.  $B_k^0$  is the maximum intensity of the pules. The parameters used are shown in Table I.

where  $\Theta(t)$  is given by

$$\tan \Theta(t) = \frac{\Omega_p(t)}{\Omega_S(t)}. \quad (11)$$

Because the Stokes pulse precedes the pump pulse,  $\Omega_p \ll \Omega_S$  and  $|\phi_0\rangle = |1, \downarrow\rangle$  at the initial time,  $T_1$ , of step II;  $\Omega_S \gg \Omega_S$  and  $|\phi_0\rangle = |3, \downarrow\rangle$  at the final time,  $T_2$ , of step II. The STIRAP control is robust to the change in the profile of the  $B_k^{(e)}$ .

### Shortcuts to adiabaticity

Assisted adiabatic transformation or shortcut-to-adiabaticity (STA) protocols have been developed to generate the same target state as reference adiabatic dynamics, with overall weaker driving fields and/or in a shorter time [30, 31]. The STA protocols have been utilised for manipulations of, e.g., isolated atoms and molecules [62–66], spin systems [67–70], Bose-Einstein condensates [71–78] and electron spin of a single nitrogen-vacancy center in diamond [79, 83]. Several STA protocols have been applied to STIRAP systems, for example Loop



STIRAP [80], counter-diabatic [62, 63], fast-forward [81] and invariant-based engineering protocols [32].

We show that the STA protocol can be used for the spin-selective transfer faster than the STIRAP control and more robust than the  $\pi$ -pulse control using the invariant-based engineering protocol [32]. The magnetic fields are represented as

$$\begin{aligned} B_{\text{p}}^{(e)}(t) &= \frac{4\hbar(\dot{\beta} \cot \gamma \sin \beta + \dot{\gamma} \cos \beta)}{g\mu_{\text{B}}\mu_{\text{p}}}, \\ B_{\text{S}}^{(e)}(t) &= \frac{4\hbar(\dot{\beta} \cot \gamma \cos \beta - \dot{\gamma} \sin \beta)}{g\mu_{\text{B}}\mu_{\text{S}}}, \end{aligned} \quad (12)$$

where

$$\begin{aligned} \gamma &= \sum_{j=0}^4 a_j t^j, \\ \beta &= \sum_{j=0}^3 b_j t^j, \end{aligned} \quad (13)$$

with  $a_0 = \varepsilon$ ,  $a_1 = 0$ ,  $a_2 = 16(\delta - \varepsilon)/T_f^2$ ,  $a_3 = -32(\delta - \varepsilon)/T_f^3$ ,  $a_4 = 16(\delta - \varepsilon)/T_f^4$ ,  $b_0 = b_1 = 0$ ,  $b_2 = 3\pi/(2T_f^2)$  and  $b_3 = -\pi/(T_f^3)$ . Here,  $T_f = T_2 - T_1$  is the duration of the control;  $\varepsilon$  and  $\delta$  determine the profile of  $B_k^{(e)}$ ;  $\varepsilon$  also determines the fidelity when there is no noise;  $\delta$  determines the population of intermediate state during the control.

## NUMERICAL RESULTS

We examine the efficiency of the level transfer in step II using a one-dimensional model for Dot 4 illustrated in Fig. 3 with the Hamiltonian:

$$H = \frac{p^2}{2m^*} + V(z) + g\mu_{\text{B}}\mathbf{B} \cdot \mathbf{S}, \quad (14)$$

where  $m^*$  is the effective electron mass and  $\mathbf{S}$  is the electron spin. We assume that the confinement of the electron in the  $xy$ -plane is sufficiently stronger than that in the  $z$  direction for simplicity. We take the potential of Dot 4 as

$$V(z) = \begin{cases} V_4 \sin^2(\pi z/L_4) & \text{for } |z| \leq L_4/2, \\ V_4 & \text{for } |z| > L_4/2. \end{cases} \quad (15)$$

Here,  $L_4$  is the width of the dot, and the depth of the potential well is  $V_4$ . The square of the amplitude of the wave functions of the three lowest levels with either spin up or down are shown in Fig. 3.

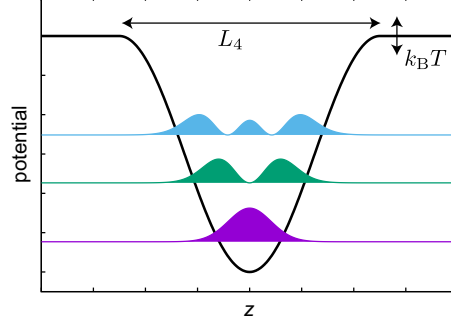


FIG. 3. Potential profile of Dot 4. The colors show the square of the amplitude of the wave functions of the three lowest levels with either spin up or down. The vertical arrows depict the fluctuation of  $V_4$  with the order of  $k_B T$ .

The dynamics of the system in step II is simulated using the three-level model expanded by  $|1, \downarrow\rangle, |2, \uparrow\rangle, |3, \downarrow\rangle$  for  $T_1 \leq t \leq T_2$  without RWA. In the numerical simulation, we solve the time-dependent Schrödinger equation with a fourth-order Runge-Kutta integrator with the time step of approximately 1 ps. The frequencies of the AC magnetic fields are  $f_p = \omega_p/(2\pi) \simeq 47$  GHz and  $f_s = \omega_s/(2\pi) \simeq 32$  GHz for  $g = 2$ ,  $L_4 = 335$  nm,  $V_4 = 0.72$  meV,  $B_z = 0.2$  T and  $m^* = 0.28m_e$ , where  $m_e$  is the electron mass. The overlapping factors are  $\mu_p = -0.05$  and  $\mu_s = -0.078$  corresponding to  $r_l = 1.4L_4$  and  $\theta_l \simeq \pi/3$ . The eigenenergies are calculated by using the Hamiltonian (14). Figure 4a shows the time-dependence of the populations of  $|1, \downarrow\rangle, |2, \uparrow\rangle$  and  $|3, \downarrow\rangle$  in the non-adiabatic spin-selective electron transfer with  $\pi$ -pulse fields, where the state is driven to  $|2, \uparrow\rangle$  and subsequently to  $|3, \downarrow\rangle$ . The parameters used are shown in Table I(a). Figure 4b shows the populations under the spin-STIRAP for the parameters in Table I(b). The population is almost directly transferred to  $|3, \downarrow\rangle$ . The finite population of  $|2, \uparrow\rangle$  around  $t = (T_p + T_s)/2$  is due to the finite pulse area. The duration of the control,  $T_2 - T_1$ , for non-adiabatic transfer is 22 times shorter than that of the spin-STIRAP. Figure 4c shows the populations in the invariant-based engineering protocol. The population of  $|2, \uparrow\rangle$  during the control depends on  $\delta$ . The duration of the control,  $T_2 - T_1$ , is 6 times shorter than that of the spin-STIRAP. The same value of  $B_k^0$  was used for these protocols.

Non-adiabatic transfer schemes take shorter time than the STIRAP transfer scheme. However the STIRAP transfer is much more robust against the error of the pulse envelope [28]. To examine the robustness of the controls against the error of the pulse profile, we

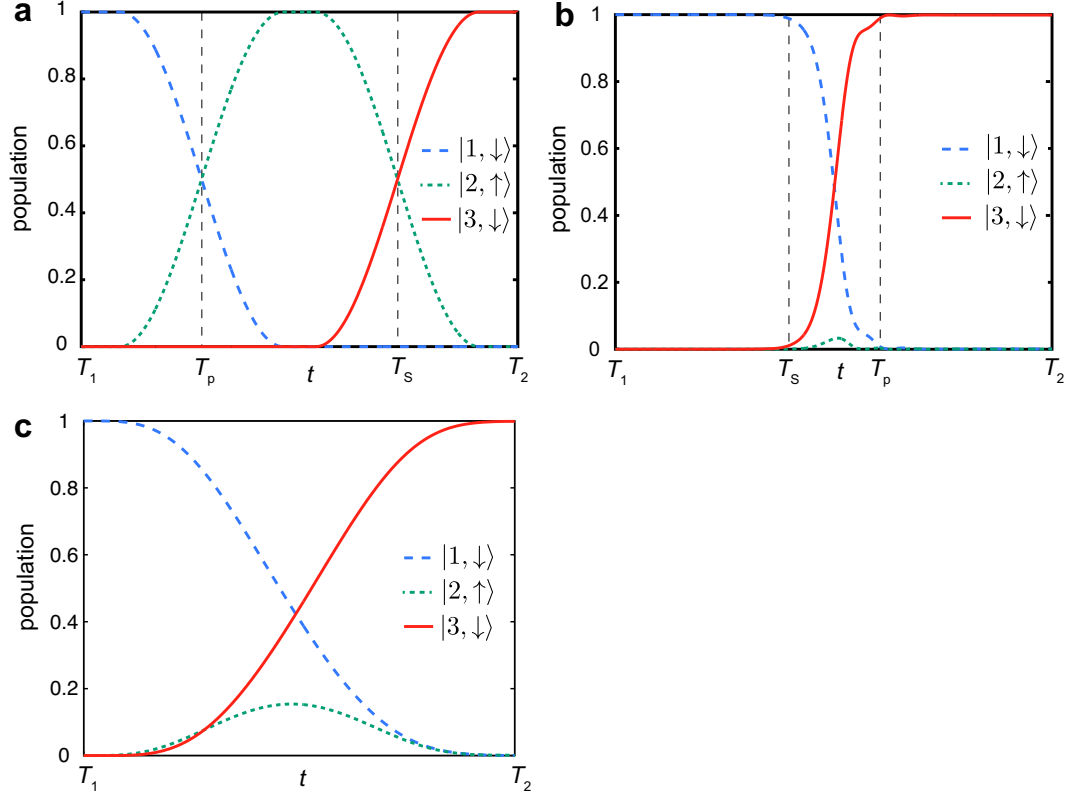


FIG. 4. Time-dependence of the populations in (a)  $\pi$  pulse control, (b) spin-STIRAP, (c) invariant-based engineering protocol. The parameters used are shown in Table I.

(a) $\pi$ pulse control		
$T_2 - T_1$	$T_S - T_p$	$\tau_k$
$17.6 \mu s$	$8.55 \mu s$	$7.13 \mu s$
(b) Spin-STIRAP		
$T_2 - T_1$	$T_p - T_S$	FWHM
$396 \mu s$	$80 \mu s$	$88 \mu s$
(c) Invariant-based engineering protocol		
$T_2 - T_1$	$\delta$	$\varepsilon$
$62 \mu s$	$\pi/8$	$0.02$

TABLE I. Parameters of the pulse fields for the spin-selective, inter-level population transfer in step II. Other parameters are given as  $B_p^0 = 0.1$  mT,  $B_S^0 = 0.064$  mT,  $f_p = 47$  GHz and  $f_S = 32$  GHz.

multiply the pump field and the Stokes field by  $\lambda_p$  and  $\lambda_s$ , respectively. Figures 5a, b and c show the dependence of the fidelity defined by the population of  $|3, \downarrow\rangle$  at  $t = T_2$  on  $\lambda_k$  for the  $\pi$ -pulse control, the spin-STIRAP and the invariant-based engineering protocol, respectively. It is seen that the spin-STIRAP and the invariant-based engineering protocols are more robust against the error of the pulse area compared to the  $\pi$ -pulse control. The spin-STIRAP shows its robustness even when the pulse area is considerably large as shown in Fig. 5b. The invariant-based engineering protocol is more robust than the  $\pi$ -pulse control especially for the case of  $\lambda_p \simeq \lambda_s$  as shown in Fig. 5c. Figure 5d shows the dependence of the fidelity of the  $\pi$ -pulse control and the invariant-based engineering protocol for  $\lambda_p = \lambda_s$ . The robustness of the invariant-based engineering protocol depends on the parameter  $\delta$ .

The fluctuation of the potential of Dot 4 can degrade the control efficiency of step II. We consider the fluctuation of  $V_4$  in equation (15). The change in  $E_i$  due to the change in  $V_4$  is about one magnitude smaller than the change of  $V_4$ . To examine the influence of the potential fluctuation we introduce the fluctuation of the energy levels  $\delta E_i$ , where  $\delta E_i$  is the modulation of the energy from the value without potential fluctuation. We model the fluctuation,  $\delta E_i$ , as a noise with a Gaussian distribution with the standard deviation  $\sigma = k_B T / 10$  and time autocorrelation function  $\alpha$ . The fluctuations of the energy levels are assumed to be independent of each other for simplicity. The time evolution of the populations were calculated by solving the time-dependent Schrödinger equation with a fourth-order Runge-Kutta integrator with the time step of approximately 1 fs. The other parameters used are shown in Table I. In the case with the level fluctuations, the total population of the states decreases to approximately 0.99 because of numerical error. The fidelity is defined by the renormalized population of  $|3, \downarrow\rangle$ . It is seen that the fidelity of the three protocols is higher than 0.995 for  $T = 100$  mK and  $\alpha = 1$  ps.

To simulate step IV, we consider the one-dimensional model of the in-line dots with the rectangular potential illustrated in Fig. 6a. Here,  $V_{bi}$  for  $i = 1, 2, 3, 4$  are the barrier potentials, and  $V_{dj}$  for  $j = 1, 2, 3$  are the potential depth of the dots. The width of the dots  $L_d$  and the width of the barriers  $L_b$  are all taken to be 30 nm. At the initial time of step IV,  $t = T_3$ , we take  $V_{b2,3} = V_{dj} = 0 < V_{b1,4}$  so that the three dots are combined and form a single larger dot. The middle barrier potentials  $V_{bi}$  and dot potentials  $V_{di}$  for  $i = 1, 2$  are

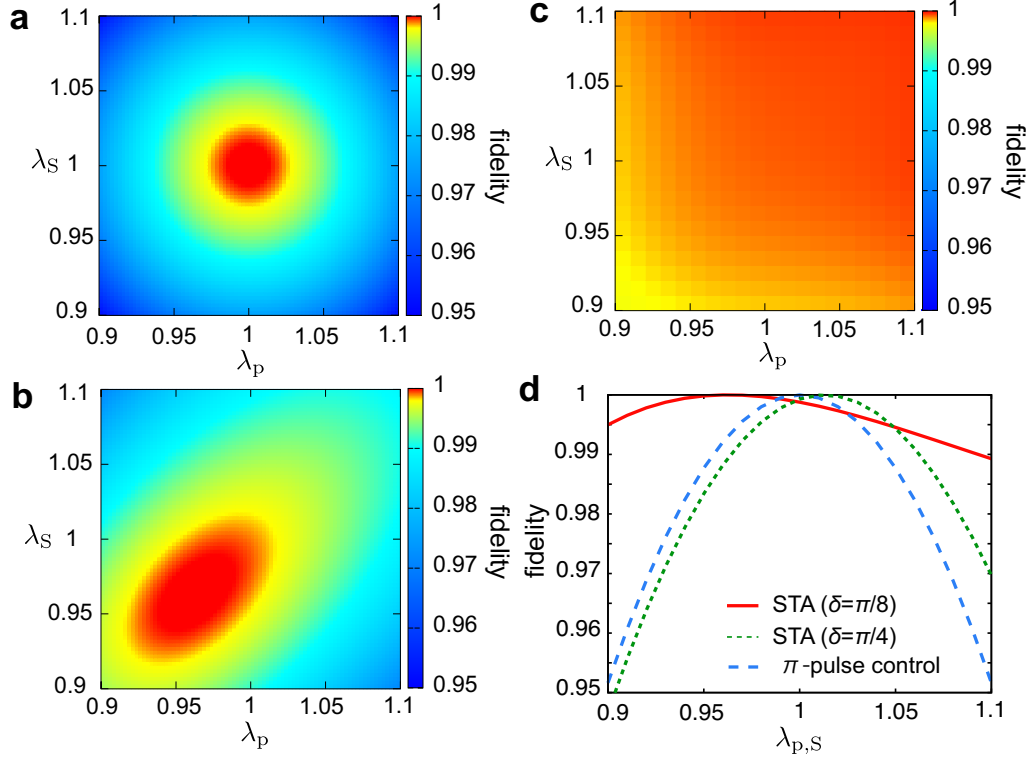


FIG. 5. Dependence of the fidelity defined by the population of  $|3, \downarrow\rangle$  at  $t = T_2$  on  $\lambda_k$  for (a)  $\pi$ -pulse control, (b) spin-STIRAP, (c) invariant-based engineering protocol. (d) The dependence of the fidelity of the  $\pi$ -pulse control and the invariant-based engineering protocol (STA) for  $\lambda_p = \lambda_s$ . The parameters used are shown in Table I. The green dotted curve and the red solid curve correspond to the STA with  $\delta = \pi/4$  and  $\delta = \pi/8$ , respectively. The blue dashed curve corresponds to the  $\pi$ -pulse control.

adiabatically increased from 0 to  $V_{bi}^{(0)}$  and  $V_{di}^{(0)}$ , respectively, as

$$V_{bi,di} = V_{bi,di}^{(0)}[R(t - T_3)], \quad T_3 \leq t \leq T_4 \quad (16)$$

with  $R(t) = [t - \sin(\omega_4 t)/\omega_4]/(T_4 - T_3)$  and  $\omega_4 = 2\pi/(T_4 - T_3)$ , while the other potentials are stationary,  $V_{b1,4} = V_{b1,4}^{(0)}$  and  $V_{d1} = V_{d1}^{(0)}$ , where  $T_4$  is the final time of step IV.  $R$  interpolates 0 to 1 smoothly with  $R(T_3) = 0$ ,  $R(T_4) = 1$  and  $R'(T_3) = R'(T_4) = 0$ , where a prime denotes time derivative. Figure. 6b shows the time-evolution of the square of the amplitude of the wave function for the initial state  $|3, \downarrow\rangle$ , which is the second excited state with spin down in the combined in-line dots. It is seen that the wave function is mostly located at Dot 3 at  $t = T_4$ . We confirmed that the state remains in the same energy level, and unwanted

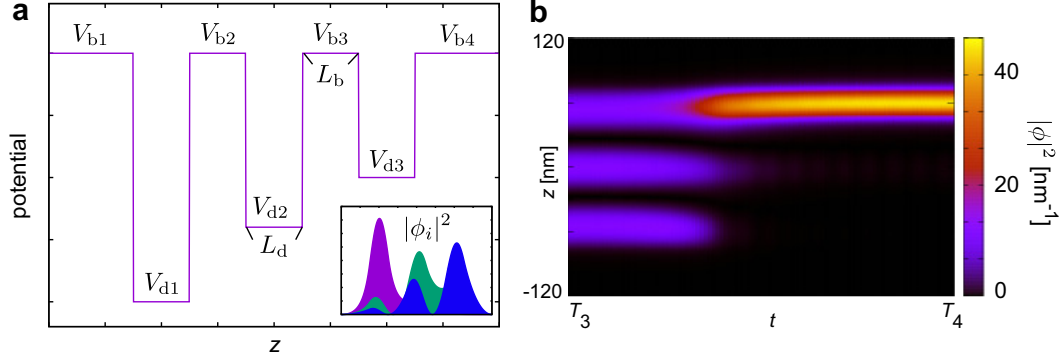


FIG. 6. (a) Schematics of the one-dimensional model of the in-line dots. The height of the potential barriers and the depth of the potential wells are denoted by  $V_{bi}$  and  $V_{dj}$  for  $i = 1, 2, 3, 4$  and  $j = 1, 2, 3$ , respectively. The inset shows the square of the amplitude of the wave function of the instantaneous eigenstates. The purple, green and blue colors correspond to  $\phi_1$ ,  $\phi_2$ , and  $\phi_3$ , respectively. (b) The time-evolution of the square of the amplitude of the wave function for the parameter set,  $V_{d1}^{(0)} = 0$ ,  $V_{d2}^{(0)} = 179 \mu\text{eV}$ ,  $V_{d3}^{(0)} = 299 \mu\text{eV}$  and  $V_{b1,2,3,4}^{(0)} = 3.6 \text{ meV}$ . The initial state is  $|3, \downarrow\rangle$ .

non-adiabatic transitions are negligible for  $T_4 - T_3 > 0.26 \text{ ns}$ .

## TWO ELECTRON TRANSPORT AND NONLOCAL OPERATION

We consider the two-electron spin-selective transfer in the system depicted in Fig. 7a to show that our protocol may be applicable to implement two-qubit gates. We assume that an electron is trapped in Dot 1 and another electron is trapped in Dot 1' at the initial time. The barrier potential between Dots 3 and 3' is sufficiently high so that the two electrons cannot pass each other. We aim to transfer the right electron to Dot 3' only when both electron spins are down initially.

The schematics of the spin-selective electron transfer is shown in Fig. 7b. We first transfer the left electron to Dot 3. We can use the method of the single electron transfer introduced above by taking into account the modulations of the overlapping factors and the resonance frequencies of the pump and the Stokes fields caused by the interaction between the electrons. The left electron is transferred only if the electron spin is down.

Now we consider the right electron transfer. First, the right electron is transferred to

Dot 4' adiabatically. When the left electron is trapped in Dot 3 or equivalently if the electron spin is down initially, the effective potential for the right electron is deformed due to the interaction with the left electron in Dot 3 more than the case in which the left electron is trapped in Dot 1 or equivalently its spin is up initially. Thus, the resonance frequencies of the pump and the Stokes fields depend on the initial spin of the left electron. This property allows us to transfer the right electron depending on the initial set of the spins. Again, we can use either of the non-adiabatic and the adiabatic schemes to transfer the right electron to Dot 3'.

This multi-electron transfer scheme can be used for non-local operations of qubits. In the end of the the control discussed above, the right electron is trapped in Dot 3' only if both of the initial electron spins are down. For example, pulsing the gate voltage of Dot 3' can realize the non-local control of the phase of the qubits' state. The phase is tuned by the pulse intensity and the duration of the pulse. The electrons are brought back to the original dots (Dot 1 and Dot 1') by the inverse electron transfer process.

The spin dependent phase in our scheme can be employed to implement important two-qubit gates, including the CNOT (Controlled NOT) gate and the CZ (Controlled Phase) gate, for quantum circuit design [84, 85]. Let us denote  $|\uparrow\rangle$  and  $|\downarrow\rangle$  as  $|0\rangle$  and  $|1\rangle$ , respectively. The above protocol implements the gate

$$U_\varphi = \begin{pmatrix} 1 & 0 & 0 & 0 \\ 0 & 1 & 0 & 0 \\ 0 & 0 & 1 & 0 \\ 0 & 0 & 0 & e^{i\varphi} \end{pmatrix}, \quad (17)$$

up to an overall phase that we can safely ignore. Here,  $\varphi$  is the phase acquired when both electrons are in the spin state  $|1\rangle$ , and the basis vectors are arranged in the order of  $|00\rangle$ ,  $|01\rangle$ ,  $|10\rangle$  and  $|11\rangle$ . The phase is controlled by manipulating the gate voltage of Dot 3'. Suppose that we adjust the parameters so that  $\varphi = \pm\pi$ . Then, we obtain the CZ gate

$$U_{\text{CZ}} = |0\rangle\langle 0| \otimes I + |1\rangle\langle 1| \otimes \sigma_z. \quad (18)$$

The CNOT gate is obtained by applying the Hadamard gate before and after the operation of the CZ gate,

$$\begin{aligned} U_{\text{CNOT}} &= (I \otimes H_{\text{Had}}) U_{\text{CZ}} (I \otimes H_{\text{Had}}) \\ &= |0\rangle\langle 0| \otimes I + |1\rangle\langle 1| \otimes \sigma_x, \end{aligned} \quad (19)$$

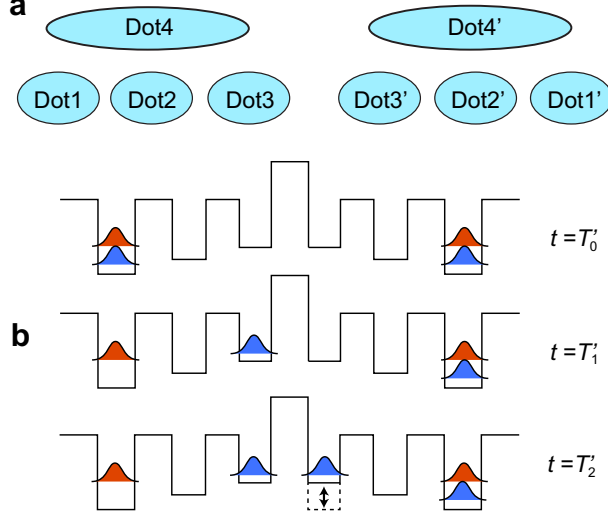


FIG. 7. (a) Schematics of the system. The conducting lead for the AC current is not depicted here. Dot 4 and Dot 4' are used for transport of the left electron and the right electron, respectively. (b) Schematics of the two-qubit gate operation. The black lines represent the potential of Dot  $i$  and Dot  $i'$  for  $i = 1, 2, 3$ . The blue and red color represent the intensity of the wave function of the spin-down and -up electrons, respectively at the initial time  $t = T'_0$ , the end of the transfer of the left electron  $t = T'_1$ ; and the end of the transfer of the right electron  $t = T'_2$ . The electrons take a superposition of spin-up and spin-down states. The right electron is transferred to Dot 3' only if the both electron spins are down initially. The arrows at Dot 3' represent the modulation of the dot potential by pulsing the gate voltage.

where

$$H_{\text{Had}} = \frac{1}{\sqrt{2}} \begin{pmatrix} 1 & 1 \\ 1 & -1 \end{pmatrix} \quad (20)$$

is the Hadamard gate. We have demonstrated that our scheme implements the universal set of gates.

## CONCLUSION

We have proposed the spin-selective, coherent electron transfer in quantum dot array. The gradient of the oscillating magnetic field and the gate voltage control are utilised to separate the electron wave function into different quantum dots depending on the electron



spin. We have examined three different protocols: the non-adiabatic  $\pi$ -pulse control, the spin-STIRAP and the invariant-based engineering protocol. The  $\pi$ -pulse control offers fast transport, and the spin-STIRAP offers a robustness of the control against the error of the pulse area of the control field although the manipulation time is longer than the  $\pi$ -pulse control. The invariant-based engineering protocol interpolates other two protocols in the sense that it is faster than spin-STIRAP and is more robust than the  $\pi$ -pulse control. We also studied the robustness of the controls to the potential fluctuation. This scheme can be extended to multi-electron systems offering the selectivity of the transport with respect to the set of spins, and can be used for non-local phase manipulation of the electrons including the CZ gate and the CNOT gate.

## ACKNOWLEDGMENT

We thank M. Möttönen for useful discussions. M.N. is grateful to JSPS for partial support from a Grants-in-Aid for Scientific Research (Grant No. 26400422). K. Y. T. acknowledges the support from the Academy of Finland (Grant No. 276528).

## AUTHOR CONTRIBUTIONS STATEMENT

S.M. and K.Y.T. came up with the initial idea for this work and developed the method. S.M. performed the simulations. M.N. improved the theory and contributed especially to the section on the two-qubit gate operations. All authors participated in the writing and revising the manuscript.

## ADDITIONAL INFORMATION

**Competing financial interests:** The authors declare no competing financial interests.

- 
- [1] Loss, D. & DiVincenzo, D. P. Quantum computation with quantum dots. *Phys. Rev. A* **57**, 120–126 (1998).

- [2] Fowler, A., Marlantoni, M., Martinis, J. M. & Cleland, A. N. Surface codes: towards practical large-scale quantum computation. *Phys. Rev. A* **86**, 032324 (2012).
- [3] Morello, A. *et al.* Single-shot readout of an electron spin in silicon. *Nature* **467**, 687–691 (2010).
- [4] Pla, J. J. *et al.* A single-atom electron spin qubit in silicon. *Nature* **489**, 541–545 (2012).
- [5] Muhonen, J. T. *et al.* Storing quantum information for 30 seconds in a nanoelectronic device. *Nat Nano* **9**, 986–991 (2014).
- [6] Maune, B. M. *et al.* Coherent singlet-triplet oscillations in a silicon-based double quantum dot. *Nature* **481**, 344–347 (2012).
- [7] Veldhorst, M. *et al.* An addressable quantum dot qubit with fault-tolerant fidelity. *Nature Nanotechnol.* **9**, 981–985 (2014).
- [8] Kawakami, E. *et al.* Electrical control of a long-lived spin qubit in a Si/SiGe quantum dot. *Nature Nanotechnol.* **9**, 666–670 (2014).
- [9] Itoh, K. M. & Watanabe, H. Isotope engineering of silicon and diamond for quantum computing and sensing applications. *MRS Commun.* **4**, 143–157 (2014).
- [10] Takeda, K. *et al.* Fault-tolerant addressable spin qubit in a natural silicon quantum dot. *Sci. Adv.* **2**, e1600694 (2016).
- [11] Harvey-Collard, P. *et al.* Nuclear-driven electron spin rotations in a single donor coupled to a silicon quantum dot. arXiv:1512.01606v1 (2015).
- [12] Veldhorst, M. *et al.* A two-qubit logic gate in silicon. *Nature* **526**, 410–414 (2015).
- [13] Kouwenhoven, L. P., Johnson, A. T., van der Vaart, N. C., Harmans, C. J. P., M. & Foxon, C. T. Quantized current in a quantum-dot turnstile using oscillating tunnel barriers. *Phys. Rev. Lett.* **67**, 1626 (1991).
- [14] Blumenthal, M. D. *et al.* Gigahertz quantized charge pumping *Nat. Phys.* **3**, 343–347 (2007).
- [15] Jehl, X. *et al.* Hybrid metal-semiconductor electron pump for quantum metrology. *Phys. Rev. X* **3**, 021012 (2013).
- [16] Connolly, M. R. *et al.* Gigahertz quantized charge pumping in graphene quantum dots. *Nat. Nanotechnol.* **8**, 417–420 (2013).
- [17] Rossi A, *et al.* An accurate single-electron pump based on a highly tunable silicon quantum dot. *Nano Lett.* **14**, 3405–3411 (2014).

- [18] Pekola, J. *et al.* Single-electron current sources: Toward a refined definition of the ampere. *Rev. Mod. Phys.* **86**, 1421 (2013).
- [19] Tantt, T. *et al.* Electron counting in a silicon single-electron pump. *New J. Phys.* **17**, 103030 (2015).
- [20] Chan, K. W. *et al.* Single-electron shuttle based on a silicon quantum dot. *Appl. Phys. Lett.* **98**, 212103 (2011).
- [21] Baart, T. A. *et al.* Single-spin CCD. *Nat. Nano.* **11**, 330–334 (2016).
- [22] Mandel, O., *et al.* Coherent transport of neutral atoms in spin-dependent optical lattice potentials, *Phys. Rev. Lett.* **91**, 010407 (2003).
- [23] Mandel, O., *et al.* Controlled collisions for multi-particle entanglement of optically trapped atoms. *Nature* **425**, 937–940 (2003).
- [24] Jaksch, D., Briegel, H.-J., Cirac, J. I., Gardiner, C. W. & Zoller, P. Entanglement of atoms via cold controlled collisions. *Phys. Rev. Lett.* **82**, 1975 (2003).
- [25] Lapasar, E. H., Kasamatsu, K., Kondo, Y., Nakahara, M. & Ohmi, T. Scalable neutral atom quantum computer with interaction on demand: Proposal for selective application of two-qubit gate. *J. Phys. Soc. Jpn.* **80**, 114003 (2011).
- [26] Lapasar, E. H. *et al.* Two-qubit gate operation on selected nearest-neighbor neutral atom qubits. *J. Phys. Soc. Jpn.* **83**, 044005 (2014).
- [27] Gaubatz, U. Rudecki, P. Schieman, S. & Bergmann, K. Population transfer between molecular vibrational levels by stimulated Raman scattering with partially overlapping laser fields. A new concept and experimental results. *J. Chem. Phys.* **92**, 5363–5376 (1990).
- [28] Bergmann, K., Theuer, H., & Shore, B. W. Coherent population transfer among quantum states of atoms and molecules. *Rev. Mod. Phys.* **70**, 1003–1025 (1998).
- [29] Vitanov, N. V., Halfmann, T., Shore, B. W., & Bergmann, K. Laser-induced population transfer by adiabatic passage techniques. *Ann. Rev. Phys. Chem.* **52**, 763–809 (2001).
- [30] Torrontegui, E. *et al.* Shortcuts to adiabaticity. *Adv. Atom. Mol. Opt. Phys.* **62**, 117–169 (2013).
- [31] Masuda, S. & Rice, S. A. Controlling quantum dynamics with assisted adiabatic processes. *Advances in Chemical Physics* **159**, (John Wiley & Sons 2016).
- [32] Chen, X. Lizuain, I., Ruschhaupt, A., Guéry-Odelin, D. & Muga, J. G. Shortcut to adiabatic passage in two- and three-level atoms. *Phys. Rev. Lett.* **105**, 123003 (2010).

- [33] Coulston, G. W. & Bergmann, K. Population transfer by stimulated Raman scattering with delayed pulses: Analytical results for multilevel systems. *J. Chem. Phys.* **96**, 3467–3475 (1994).
- [34] Martin, J., Shore, B. W., & Bergmann, K. Coherent population transfer in multilevel systems with magnetic sublevels. III. Experimental results. *Phys. Rev. A* **54**, 1556–1569 (1996).
- [35] Halfmann, T., & Bergmann, K. Coherent population transfer and dark resonances in SO<sub>2</sub>. *J. Chem. Phys.* **104**, 7068–7072 (1996).
- [36] Malinovsky, V. S. & Tannor, D. J. Simple and robust extension of the stimulated Raman adiabatic passage technique to  $N$ -level systems. *Phys. Rev. A* **56**, 4929–4937 (1997).
- [37] Kobra, M. N. & Rice, S. A. Selective photochemistry via adiabatic passage: An extension of stimulated Raman adiabatic passage for degenerate final states. *Phys. Rev. A* **57**, 2885–2894 (1998).
- [38] Kurkal, V. & Rice, S. A. Sequential STIRAP-based control of the HCN→CNH isomerization. *Chem. Phys. Lett.* **344**, 125–137 (2001).
- [39] Cheng, T., Darmawan, H., & Brown, A. Stimulated Raman adiabatic passage in molecules: The effects of background states. *Phys. Rev. A* **75**, 013411–013421 (2007).
- [40] Jakubetz, W. Limitations of STIRAP-like population transfer in extended systems: The three-level system embedded in a web of background states. *J. Chem. Phys.* **137**, 224312–224327 (2012).
- [41] Eckert, K. *et al.* Three-level atom optics via the tunneling interaction. *Phys. Rev. A* **70**, 023606 (2004).
- [42] Eckert, K., Mompert, J., Corbalán, R., Lewenstein, M. & Birkel, G. Three level atom optics in dipole traps and waveguides. *Opt. Commun.* **264**, 264–270 (2006).
- [43] Opatrný, T. & Das, K. K. Conditions for vanishing central-well population in triple-well adiabatic transport. *Phys. Rev. A* **79**, 012113 (2009).
- [44] O’Sullivan, B., Morrissey, P., Morgan, T. & Busch, Th. Using adiabatic coupling techniques in atom-chip waveguide structures. *Phys. Scr. T* **140**, 014029 (2010).
- [45] Morgan, T., O’Sullivan, B., & Busch, Th. Coherent adiabatic transport of atoms in radio-frequency traps. *Phys. Rev. A* **83**, 053620 (2011).
- [46] Morgan, T., O’Riordan, L. J., Crowley, N., O’Sullivan, B. & Busch, Th. Coherent transport by adiabatic passage on atom chips. *Phys. Rev. A* **88**, 053618 (2013).

- [47] Greentree, A. D., Cole, J. H., Hamilton, A. R. & Hollenberg, L. C. L. Coherent electronic transfer in quantum dot systems using adiabatic passage. *Phys. Rev. B* **70**, 235317 (2004).
- [48] Jong, L. M. *et al.* Coherent tunneling adiabatic passage with the alternating coupling scheme. *Nanotechnology* **20**, 405402 (2009).
- [49] Graefe, E. M., Korsch, H. J. & Witthaut, D. Mean-field dynamics of a Bose-Einstein condensate in a time-dependent triple-well trap: Nonlinear eigenstates, Landau-Zener models, and stimulated Raman adiabatic passage. *Phys. Rev. A* **73**, 013617 (2006).
- [50] Rab, M. *et al.* Spatial coherent transport of interacting dilute Bose gases. *Phys. Rev. A* **77**, 061602 (2008).
- [51] Nesterenko, V. O., Novikov, A. N., de Souza Cruz, F. F. & Lapolli, E. L. STIRAP transport of Bose-Einstein condensate in triple-well trap. *Laser Phys.* **19**, 616–624 (2009).
- [52] Rab, M., Hayward, A. L. C., Cole, J. H., Greentree, A. D. & Martin, A. M. Interferometry using adiabatic passage in dilute-gas Bose-Einstein condensates. *Phys. Rev. A* **86**, 063605 (2012).
- [53] Dittmann, P. *et al.* The effect of vibrational excitation ( $3 \leq \nu' \leq 19$ ) on the reaction  $\text{Na}_2(\nu') + \text{Cl} \rightarrow \text{NaCl} + \text{Na}^*$ . *J. Chem. Phys.* **97**, 9472–9475 (1992).
- [54] Kulin, S. *et al.* Coherent manipulation of atomic wave packets by adiabatic transfer. *Phys. Rev. Lett.* **78**, 4185 (1997).
- [55] Longhi, S., Della Valle, G., Ornigotti, M. & Laporta, P. Coherent tunneling by adiabatic passage in an optical waveguide system. *Phys. Rev. B* **76**, 201101 (2007).
- [56] Lahini, Y. *et al.* Effect of nonlinearity on adiabatic evolution of light. *Phys. Rev. Lett.* **101**, 193901 (2008).
- [57] Menchon-Enrich, R., Llobera, A., Cadarso, V. J., Mompart, J. & Ahufinger, V. Adiabatic passage of light in CMOS-compatible silicon oxide integrated Rib waveguides. *IEEE Photonics Technol. Lett.* **24**, 536–538 (2012).
- [58] Menchon-Enrich, R. *et al.* Light spectral filtering based on spatial adiabatic passage. *Light: Sci. Appl.* **2**, e90. (2013).
- [59] Menchon-Enrich, R., Mompart, J. & Ahufinger, V. Spatial adiabatic passage processes in sonic crystals with linear defects. *Phys. Rev. B* **89**, 094304 (2014).
- [60] Kumar, K. S. *et al.* Stimulated Raman adiabatic passage in a three-level superconducting circuit. *Nat. Commun.* **7**, 10628; 10.1038/ncomms10628 (2016).

- [61] Hollenberg, L. C. L., Greentree, A. D., Fowler, A. G. & Wellard C. J. Two-dimensional architectures for donor-based quantum computing. *Phys. Rev. B* **74**, 045311 (2006).
- [62] Demirplak, M. & Rice, S. A. Adiabatic population transfer with control fields. *J. Phys. Chem. A* **107**, 9937–9945 (2003).
- [63] Chen, X., Lizuain, I., Ruschhaupt, A., Guéry-Odelin, D. & Muga, J. G. Shortcut to adiabatic passage in two- and three-level atoms. *Phys. Rev. Lett.* **105**, 123003 (2010).
- [64] Masuda, S. & Rice, S. A. Selective vibrational population transfer using combined stimulated Raman adiabatic passage and counter-diabatic fields. *J. Phys. Chem. C* **119**, 14513–14523 (2014).
- [65] Du, Y.-X. *et al.* Experimental realization of stimulated Raman shortcut-to-adiabatic passage with cold atoms. *Nat. Commun.* **7**, 12479 (2016).
- [66] An, S., Lv, del Campo, A. & Kim, K. Shortcuts to adiabaticity by counterdiabatic driving for trapped-ion displacement in phase space. *Nat. Commun.* **7**, 12999; 10.1038/ncomms12479 (2016).
- [67] Berry, M. Transitionless quantum driving. *J. Phys. A: Math. Gen.* **42**, 365303 (2009).
- [68] del Campo, A., Rams, M. M. & Zurek, W. H. Assisted finite-rate adiabatic passage across a quantum critical point: exact solution for the quantum Ising model. *Phys. Rev. Lett.* **109**, 115703 (2012).
- [69] Fasihi, M. -A., Wan, Y. & Nakahara, M. Non-adiabatic fast control of mixed states based on Lewis-Riesenfeld invariant. *J. Phys. Soc. Jpn.* **81**, 024007 (2012)
- [70] Takahashi, K. Transitionless quantum driving for spin systems. *Phys. Rev. E* **87**, 062117 (2013).
- [71] Masuda, S. & Nakamura, K. Fast-forward of adiabatic dynamics in quantum mechanics. *Proc. R. Soc. A* **466**, 1135–1154 (2009).
- [72] Muga, J. G., Chen, X., Ruschhaupt, A. & Guéry-Odelin, D. Frictionless dynamics of Bose-Einstein condensates under fast trap variations. *J. Phys. B: At. Mol. Opt. Phys.* **42**, 241001 (2009).
- [73] Schaff, J.-F., Song, X.-L., Capuzzi, P., Vignolo, P. and Labeyrie, G. Shortcut to adiabaticity for an interacting Bose-Einstein condensate. *EPL*, **93**, 23001 (2011).
- [74] Bason, M. G. *et al.* High-fidelity quantum driving. *Nat. Phys.* **8**, 147–152 (2011).

- [75] Masuda, S. Acceleration of adiabatic transport of interacting particles and rapid manipulations of a dilute Bose gas in the ground state. *Phys. Rev. A* **86**, 063624 (2012).
- [76] Torrontegui, E., Martínez-Garaot, S., Ruschhaupt, A. & Muga, J. G. Shortcuts to adiabaticity: Fast-forward approach *Phys. Rev. A* **86**, 013601 (2012).
- [77] Deffner, S., Jarzynski, C. & del Campo, A. Classical and quantum shortcuts to adiabaticity for scale-invariant driving *Phys. Rev. X* **4**, 021013 (2014).
- [78] Masuda, S., Nakamura, K. & del Campo, A. High-fidelity rapid ground-state loading of an ultracold gas into an optical lattice. *Phys. Rev. Lett.* **113**, 063003 (2014).
- [79] Zhou, B. B. *et al.* Accelerated quantum control using superadiabatic dynamics in a solid-state lambda system. arXiv:1607.06503 (2016).
- [80] Unanyan, R. G., Yatsenko, L. P., Bergmann, K. & Shore, B. W. Laser-induced adiabatic atomic reorientation with control of diabatic losses. *Opt. Commun.* **139**, 48–54 (1997).
- [81] Masuda, S. & Rice, S. A. Fast-forward assisted STIRAP. *J. Phys. Chem. A* **119**, 3479–3487 (2015).
- [82] Yang, C. H. *et al.* Spin-valley lifetimes in a silicon quantum dot with tunable valley splitting. *Nat. Commun.* **4**, 2069; 10.1038/ncomms3069 (2013).
- [83] Zhang, J. *et al.* Experimental implementation of assisted quantum adiabatic passage in a single spin. *Phys. Rev. Lett.* **110**, 240501 (2013).
- [84] Nielsen, M. A. & Chuang, I. L. *Quantum computation and quantum information*. (Cambridge Univ. Press, 2000).
- [85] Nakahara, M. & Ohmi, T. *Quantum computing: from linear algebra to physical realizations*. (CRC Press, 2008).